


## Research Article

# Galvanic Corrosion and Fatigue Behavior of a SM480C Welded Joint Steel in a Sea-Crossing Suspension Bridge

Xudong Zhou,<sup>1</sup> Xinmin Zhang,<sup>1</sup> Ruiwen Xu,<sup>1</sup> Bin Li,<sup>2</sup> Xuechong Ren ,<sup>2</sup> Jinyang Zhu,<sup>2</sup> and Ying Jin<sup>2</sup>

<sup>1</sup>Guangdong Highway Construction Co. Ltd, No. 32, Zhujiang East Road, Zhujiang New Town, Tianhe District, 510630 Guangzhou, China

<sup>2</sup>National Center for Material Service Safety, University of Science & Technology Beijing, No. 30 Xueyuan Road, Haidian District, 100083 Beijing, China

Correspondence should be addressed to Xuechong Ren; [ustbrenxuechong@163.com](mailto:ustbrenxuechong@163.com)

Received 20 May 2022; Revised 2 July 2022; Accepted 7 July 2022; Published 29 July 2022

Academic Editor: Michael J. Schütze

Copyright © 2022 Xudong Zhou et al. This is an open access article distributed under the Creative Commons Attribution License, which permits unrestricted use, distribution, and reproduction in any medium, provided the original work is properly cited.

The corrosion tendency and fatigue behavior of a SM480C welded joint in a sea-crossing suspension bridge after twenty-year exposure to a marine environment was investigated in this work. It was found that the corrosion product on the whole surface of the welded joint is loose, with many holes and cracks, which allowing corrosive media enter and reach the surface of the substrate. Localized corrosion occurred in the weld zone (WZ) and the heat-affected zone (HAZ), the maximum depth of localized corrosion in the HAZ reached 1.8 mm, and the maximum local corrosion rate is 0.082 mm/y. By using Bimetallic Conjugation Theory calculations, the galvanic effect of the welded joint was qualified, indicates that HAZ was the most corrosion susceptible area in the welded joint. The galvanic corrosion current on HAZ reached approximately  $2\ \mu\text{A}$ , which is much higher than the corrosion of isolated HAZ by about 6.5 times. The corrosion has an obvious influence on the fatigue performance, the elongation of the bridge deck decreases by 40%~70%, and the tensile strength decreases by 4.5%~31.33%. In order to ensure the service safety and avoid premature failure, the average thickness of the corroded bridge deck should not be less than 10 mm under the stress amplitude of 115 MPa.

## 1. Introduction

The beefed-up designed strength of bridge steels has been recently enhanced with the development of cross-sea bridge. This requires advanced corrosion resistance, toughness, and fatigue properties of the material. Generally, in the offshore area, the corrosion behavior of bridge deck steels usually exhibits obvious regional environment-dependent characteristics [1–4], which are affected by environmental factors such as the ocean water, oxid film [5], high sedimentation content of chloride ions [6], temperature, precipitation of secondary phases, bottom sediments, and external load stress. High-strength bridge steels are frequently subjected to severe corrosion and high fatigue loading during service [7–11]. The corrosion pits and defects caused by initial corrosion can act as crack nucleation sites and exert a negative effect on the subsequent

mechanical and fatigue properties. Therefore, the corrosion problem of welded joints became an increasingly prominent damage factor of structural constructions.

Many investigators have studied the corrosion resistance mechanism by the way of long-term atmospheric environment outdoors exposure and simulated accelerated test at laboratory simultaneously [12, 13]. Generally, it is believed that the main factor that affects the durability of bridge structures is the corrosion degrees, and with the synergistic effect of service time and load, corroded bridges are more prone to fracture failure [14–16]. According to Li et al. [17], in sodium chloride environment, pitting corrosion of high strength steel occurs firstly near the sulfide inclusion, resulting in crack initiation and progressively reducing the service life. The use of simulation platform of corrosion combined with mechanical fatigue test is another straightforward and widely applied

method. Y. S. Kim and J. G. Kim [18], for example, have investigated the influence of corrosion on the mechanical behavior of the welded joint pipe by combining corrosion simulation with mechanical simulation. The result shows that the welded joint is preferentially corroded due to the serious corrosion factors, and the corrosion rate is high when exposed to the external environment. The stress concentration phenomenon on the welded joint of corroded samples increased with exposure time, indicating that the failure risk of the welded joint had a positive correlation to the increase of corrosion degradation. In addition, several studies have been conducted on the galvanic interaction of welded joints. Based on these studies [19], it can be inferred that apart from the potential differences between the area of welded joints, other factors (ion concentration/temperature/depth of solution film) also played important roles in the galvanic interaction of welded joints. In the work of Xu and Wang [20], it was observed that the corrosion of high strength low alloy steel (HSLA) and laser welded hot stamping ultrahigh strength steel (UHSS) in 0.017 M NaCl solution mainly occurs in the UHSS matrix. This phenomenon was ascribed to the current effect caused by the potential difference of 200 mV between UHSS and OCP. Considering the increased usage amount of UHSS, the localized corrosion caused by UHSS may reduce the fatigue performance. Hence, corrosion fatigue crack initiation and propagation could be greatly accelerated, resulting in a significant decline of fatigue life [21–26]. Therefore, the corrosion behavior of bridge steel in this environment must be studied, especially the synergy influence of the galvanic corrosion and fatigue behaviors to the welded joints.

The bridge deck is made of SM480C, which is low alloy hot-rolled structural steel with excellent weldability. The welding method is CO<sub>2</sub> automatic welding. The suspension bridge is located at the mouth of the sea, and the climate at the bridge site is subtropical marine climate, warm, and rainy all year round. The temperature is the highest in July and August and the lowest in January and February, with the average temperature range of 13.5°C to 28.7°C. In addition, the suspension bridge has been serviced for more than 20 years. In this environment, there exist a high risk of corrosion and fatigue problems. Therefore, it is necessary to investigate the corrosion fatigue resistance performance of the bridge decks to ensure the structural safety and integrity. This study provides critical information needed for the corrosion protection of the suspension bridge. A scanning electron microscope (SEM) equipped with an energy dispersive X-ray (EDX) spectrometer and three-dimensional-morphology testing analyzer (LSCM) were utilized for the microstructural characterization of the bridge deck welded joint samples. Electrochemical test methods such as open circuit potential (OCP) and potentiodynamic polarization (PDP) are employed in studying the macroscopic galvanic corrosion of the welded joints. Additionally, fatigue tests such as uniaxial tensile and strain-controlled low-cycle fatigue tests were conducted to evaluate the mechanical properties of the raw and serviced bridge decks. Moreover, this study explored and analyzed the corrosion tendency and fatigue corrosion mechanism, and the corrosion damage and health in service status of the bridge were evaluated in this article and will also provide technical support for the anticorrosion transformation of the suspension bridge.

TABLE 1: The chemical composition of SM480C steels in weight %.

Cr	Mn	Ni	Si	S	P	Fe
0.22	1.47	0.22	0.18	0.12	0.15	Balance

## 2. Materials and Methods

**2.1. Materials.** SM480C low alloy hot-rolled steel was produced by Japanese company and tailored to 100 × 100 × 12 mm size through a cutting machine. The main chemical compositions of the SM480C steel are shown in Table 1. The samples were prepared by cutting the serviced suspension bridge deck (No. 62 sling) and the bridge deck with welded joints (No. 38 sling), and the sampling location is given in Figure 1. The metallographic samples are selected from unserviceable stock bridge decks.

**2.2. Corrosion Morphology and Corrosion Layer Analysis.** The surface morphology of the sample was observed by Olympus GX-71 metallographic microscope, and the composition of the bridge deck was analyzed by X-ray diffractometer (XRD). Test conditions are as follows: Cu-K $\alpha$  source, current 30 mA, voltage 40 kV,  $10^\circ \leq 2\theta \leq 80^\circ$ , step length 0.02, and collection time 2.5 s. The micromorphology of the sample was analyzed by using EVO MA 25/LS 25 scanning electron microscopy (SEM), and the chemical and phase composition of the sample surface were characterized by using EDS (X-Flash-Detector 5010) device matching with scanning electron microscopy (SEM). The macroscopic surface and section morphology were characterized by KY-YX2010Z 3D morphometer.

**2.3. Tensile and Fatigue Test Procedure.** The tensile and fatigue specimens were taken from the actual bridge deck. The appearance of samples is shown in Figure 2. The width and the length of test section are 15 mm and 30 mm, respectively. The thickness of specimens was measured one by one because the corrosion degree of different sample surfaces is different. Constant amplitude axial fatigue tests were conducted in ambient air according to standard ASTM E466-07 with the stress ratio  $R = -1$ , and the waveform was sine wave. The tensile and fatigue specimens were tested on a W+B LFV-100 hydraulic servo test machine.

**2.4. Potentiodynamic Polarization Measurements.** The galvanic corrosion tendency of the welded joints was studied by potentiodynamic polarization curve in an electrochemical workstation (Gamry Reference 600 workstation) that had a three-electrode system, a platinum sheet as the counter electrode, and a silver-silver chloride electrode as the reference electrode. The electrochemical samples were obtained by wire cutting from the serviced bridge deck. The back of the samples were polished to the metal matrix with 240#, 400#, 800#, 1200#, and 2000# sic sandpaper. The working surface of 1 cm<sup>2</sup> was exposed to 3.5 wt % NaCl solution, and the rest were submerged by epoxy resin.

The open circuit potential and electrokinetic polarization curves of each welding area were compared and tested. The OCP of the samples was measured for 40 minutes to ensure the value reached steady state. The potentiodynamic polarization curves were measured in the potential range from

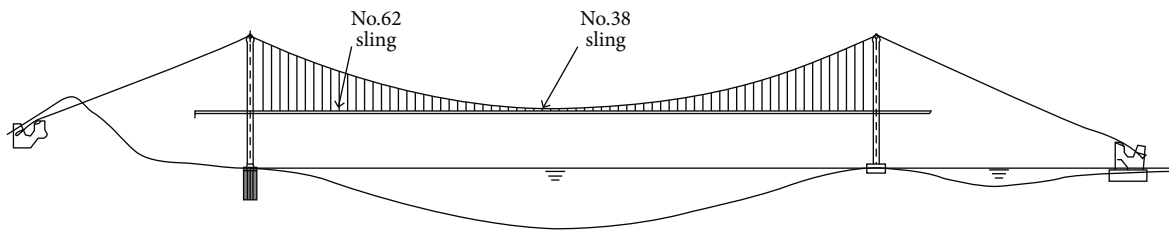


FIGURE 1: Typical bridge deck samples obtained on different site.



FIGURE 2: Appearance of a tensile and fatigue sample.

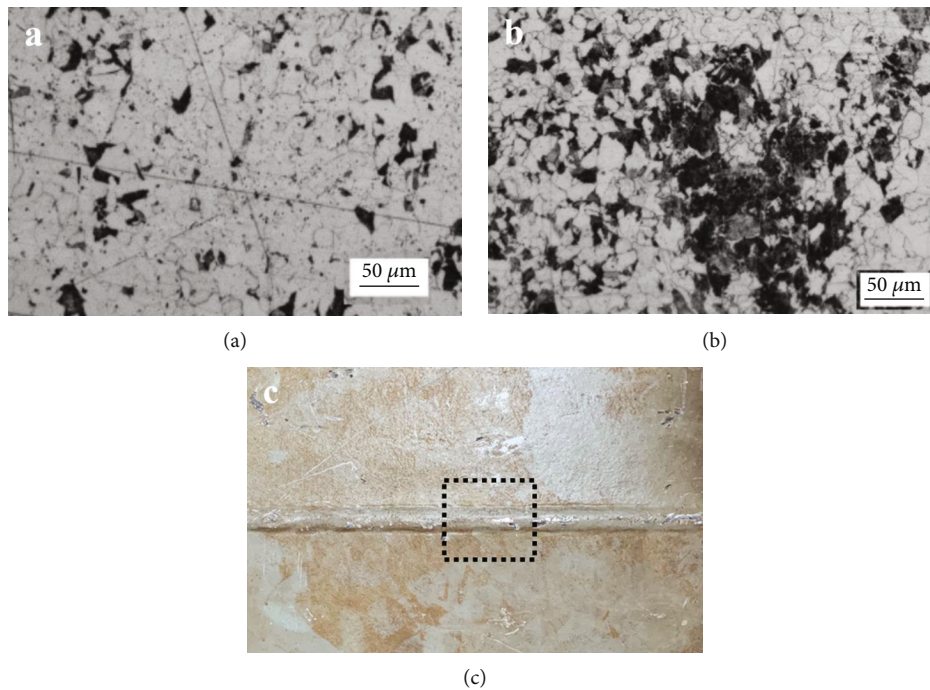


FIGURE 3: (a) Metallograph picture of the WZ; (b) metallograph picture of the HAZ; (c) sampling location of the welding area.

-300 mV, vs. OCP to +400 mV, vs. OCP, and the test rate was 20 mV/min. All tests were performed at 25°C and repeated three times to ensure repeatability.

### 3. Results

**3.1. Corrosion Morphology and Corrosion Layer Analysis.** Figure 3 illustrates the metallographic structure of each area of the bridge deck samples, including the WZ, the HAZ, and the BM. Considering the possible differences of metallographic structure in different regions, three different locations were selected for testing. It can be seen that the surface eroded by 5% nitric acid alcohol solution, compared with the plate base material area, and the microstructure of the WZ is more uniform and compact. It is obvious that the structure composed

of massive ferrite (white) and pearlite (black) can be clearly observed. Due to the high temperature of welding, the grain size in the HAZ is more coarser than that in the matrix, which indicates that there appeared grain growth phenomenon in the welding process, the uniform distribution of the whole structure is poor, and it can also found that there exists local segregation phenomenon of pearlite.

The SEM morphologies of welded joint microstructure are shown in Figure 4. Corrosion products in the WZ were strip and lamellar, while the products in the HAZ were mainly fine lamellar and slime, with distinct product film stratification. From the section photos, obvious local corrosion exists in both the WZ and HAZ, and the depth of corrosion pit in the HAZ is about 1.8 mm, indicating that the welded joint has certain corrosion risk, especially in the HAZ.



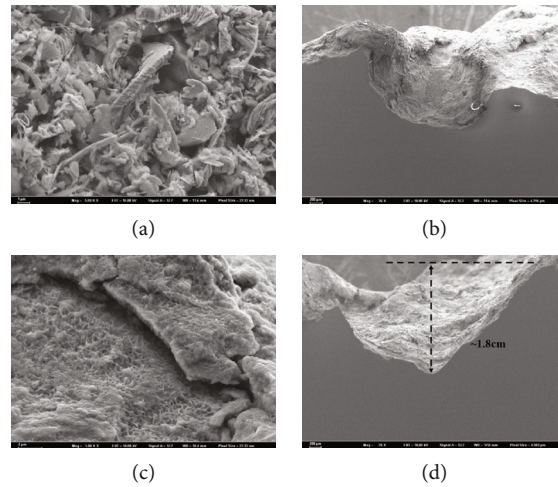


FIGURE 4: (a) SEM morphologies of the WZ; (b) cross-sectional image of the WZ; (c) SEM morphologies of the HAZ; (d) cross-sectional image of the HAZ.

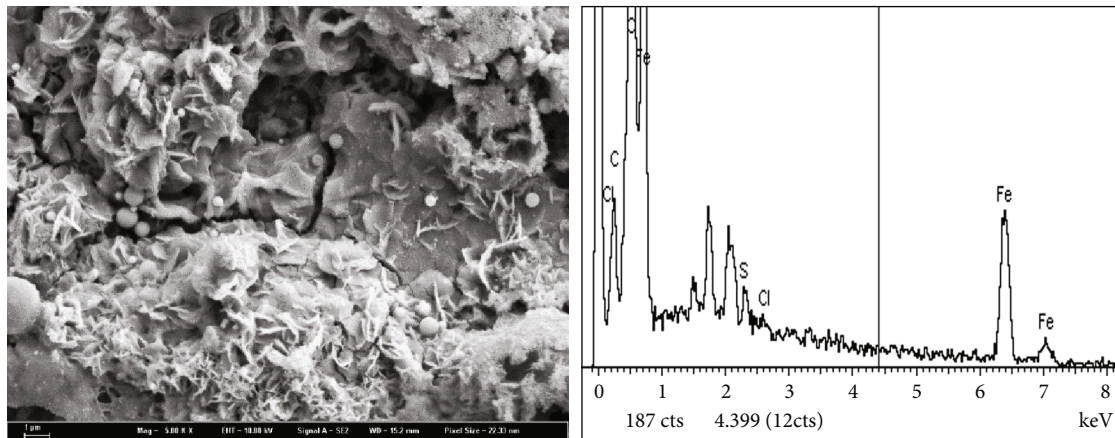


FIGURE 5: Corrosion products and EDS results of bridge deck surface.

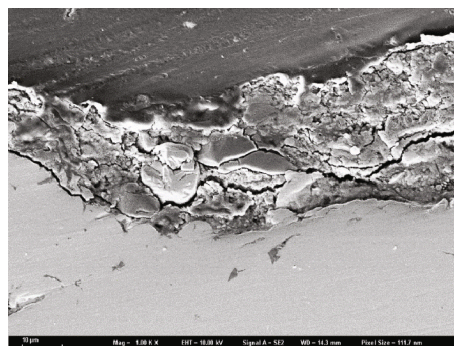
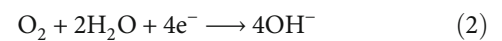


FIGURE 6: Micromorphology of the bridge deck cross section.

Figure 5 shows the micrographs and EDS spectra of the serviced bridge deck surface. For marine environment corrosion, the  $\text{Cl}^-$  is inside the corrosion pit. After the beginning of corrosion, the initial point of corrosion becomes the anodic point due to the dissolution of active iron [27].



The matrix is under the peripheral part of the droplet, serviced as the cathodic site with the occurrence of oxygen ( $\text{O}_2$ ) reduction and generation of hydroxyl ions ( $\text{OH}^-$ ).



The  $\text{Fe}^{2+}$  ions were released into the solution inside the pit and reacted with  $\text{Cl}^-$  ions that migrated to the anodic site

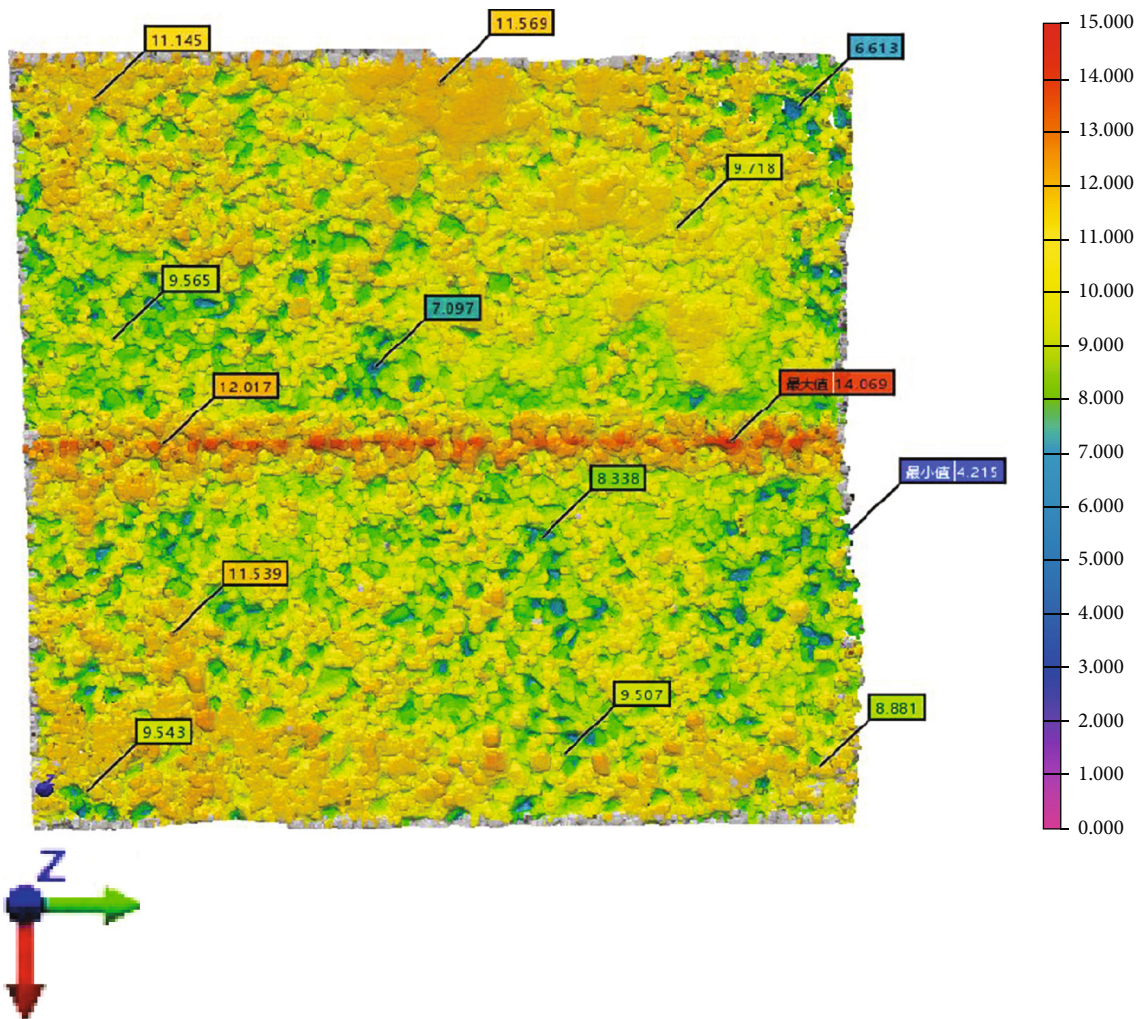


FIGURE 7: Overall thickness distribution cloud diagram of bridge deck with welded joint.

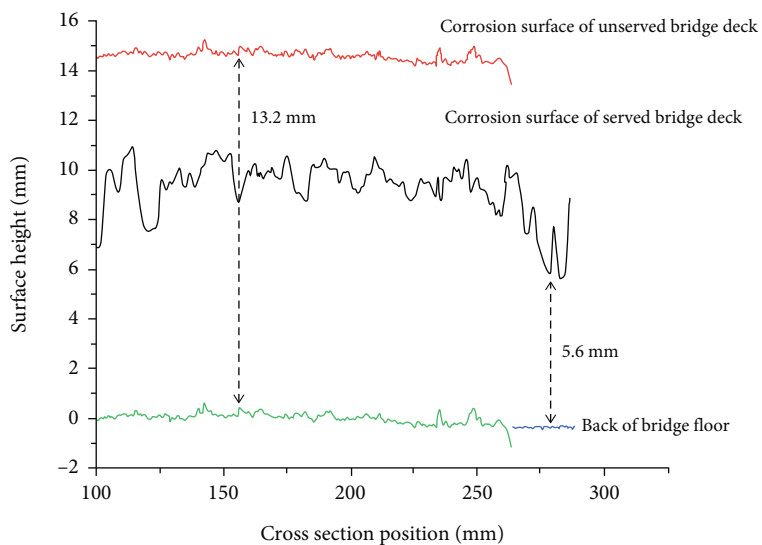


FIGURE 8: Comparison of corrosion height of bridge deck section.

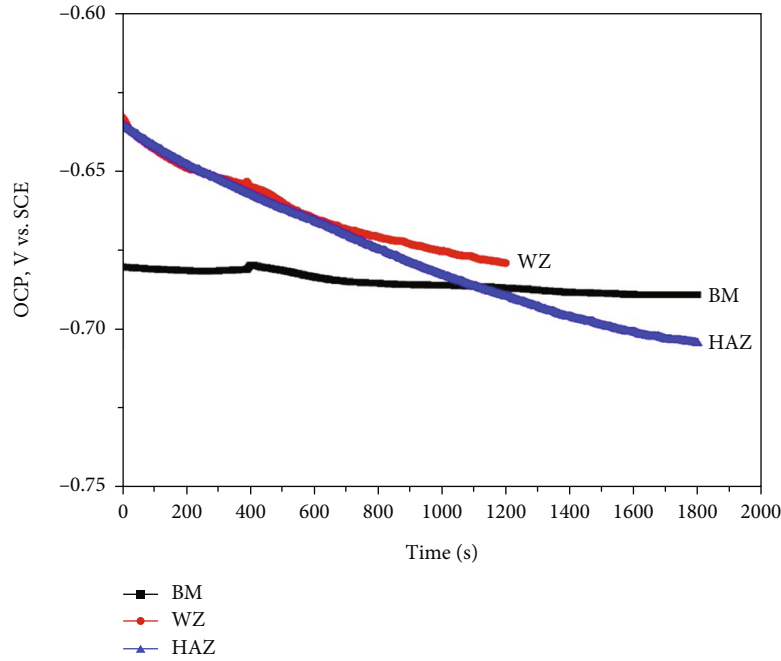


FIGURE 9: Open circuit potential in different areas of welded joints.

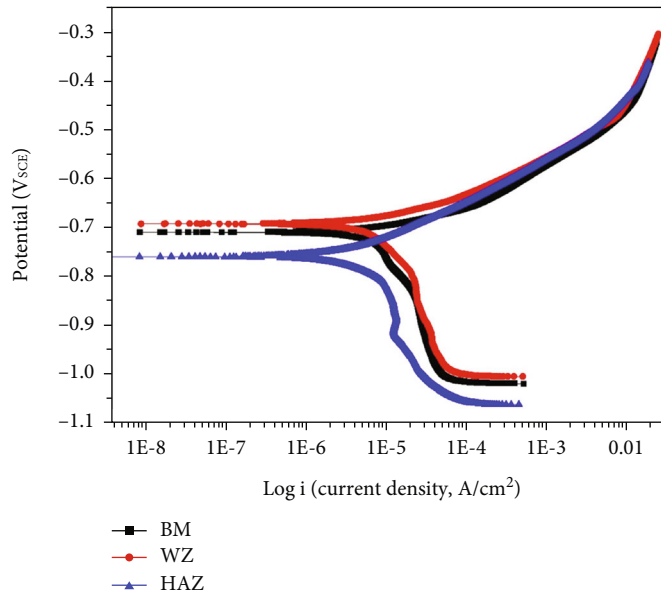
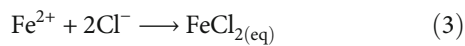
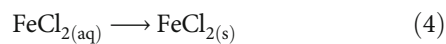


FIGURE 10: Polarization curves of welded joints in different areas.

to maintain charge neutrality, forming  $\text{FeCl}_2$ .

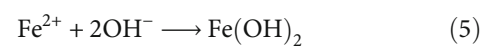


The precipitation of this highly soluble salt is given by reaction.



The  $\text{Fe}^{2+}$  ions generated in the corrosion pit reached

$\text{OH}^-$  generated forming  $\text{Fe}(\text{OH})_2$ .



$\text{Fe}(\text{OH})_2$  can further react to form other oxy-hydroxides, such as  $\alpha\text{-FeOOH}$ ,  $\gamma\text{-FeOOH}$ , and  $\delta\text{-FeOOH}$  [28, 29].

The corrosion product film formed on the surface of the bridge deck, and the morphology was loose on the whole with cracks in local parts. The EDS energy spectrum shows that the corrosion product mainly contains Fe and O and a

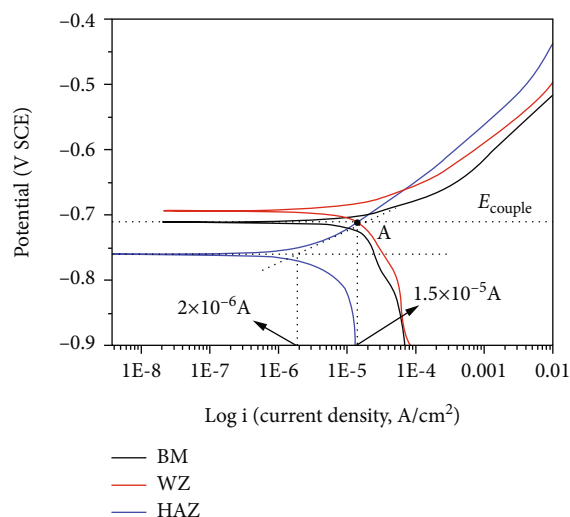


FIGURE 11: Quantization results of galvanic effect between different areas of welded joints.

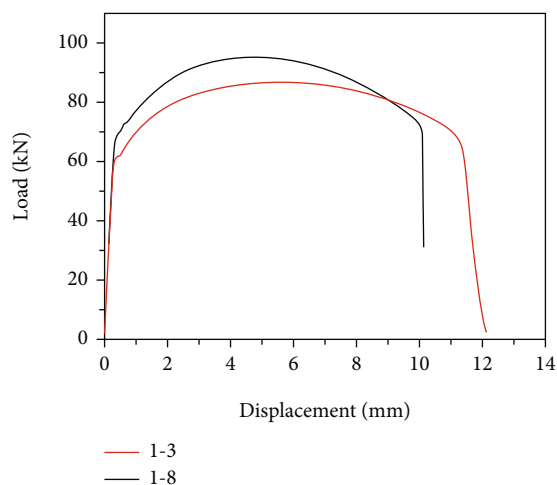


FIGURE 12: Tensile load-displacement curves of serviced bridge deck samples.

small amount of Cl, S, and Si. Among them, Fe and O mainly exist in the form of Fe oxides, such as  $\text{Fe}_2\text{O}_3$ , Cl is mainly chlorine salt brought by salt fog in marine and atmospheric environment, Si comes from dust particles in the atmosphere, and S is mainly related to sulfur elements originally contained in the metal matrix and a small amount of sulfur oxides in atmosphere.

Figure 6 shows the cross section corrosion product film layer microstructure pictures of the bridge deck. The surface layer of the suspension bridge is relatively loose, with a certain number of holes and cracks, and provides amount channel for the corrosive medium, such as oxygen, salt, and moisture, into the substrate surface. The channel is uncondusive to the protection of substrate, causing a gradually increased corrosion process in substrate during the long-term service.

Figure 7 presents the cloud diagram of the overall thickness distribution of the serviced bridge deck samples. The

overall thinning of the bridge deck is not uniform, which is obviously raised in the mediate weld zone (the red-orange area). The thinning is serious on both sides of the weld, and the remaining thickness of the maximum thinning area is about 4 mm. With the initial thickness of the bridge deck samples is 12 mm, the annual corrosion rate is 0.37 mm/y, which is in a high corrosion risk. As shown in Figure 8, a comparative analysis was made on the corroded working face and the above thickness cloud image in the cross section direction. Taking the repertory bridge deck samples as a reference, it can be seen that the overall corrosion of the bridge deck that has been in service is relatively uniform, the intermediate WZ is narrow, and the bulge is not obvious in the section height diagram. Overall, the corrosion of the suspension bridge is serious, the thickness of the maximum thinning area is only about 3~4 mm, and the annual corrosion rate is 0.3~0.4 mm/y, which has a high risk of corrosion failure. Considering the suspension bridge has been serviced for more than 20 years, it is essential to monitor the health status of the key parts and evaluate and maintain the whole corrosion damage of the bridge, so as to ensure the risk early-warning identification, with safe and reliable service of the bridge in the later service.

**3.2. Electrochemical Behavior Analysis.** The electrochemical corrosion behaviors of each zone (BM, HAZ, and WZ) were evaluated electrochemical workstation device. The OCP curves are shown in Figure 9. It tells that the open circuit potentials of samples obtained from BM, HAZ, and WZ were -0.71 V, -0.76 V, and -0.69 V, respectively. Meanwhile, the open circuit potential value of WZ and HAZ samples fluctuated greatly, while that of BM sample fluctuated little. The corrosion potential of HAZ sample is the lowest, while that of BM sample is the highest, and the potential value of WZ sample is between them, indicating that macroscopic galvanic effect of HAZ may exist in the welded joints. Then, fit the potentiodynamic polarization curves, and the results are displayed in Figure 10, using the same work area ( $1\text{ cm}^2$ ) in electrochemical test specimen. Under the premise of BM and WZ polarization curves were relatively close, the anode polarization curve of HAZ intersected the cathodic polarization curves of BM and WZ. The phenomenon implied that under the condition of the welding joint district accidentally met, the anodic dissolution in the HAZ is accelerated by the galvanic effect of the WZ and BM.

To further figure out the influence of galvanic corrosion accelerating effect on welded joints, the corrosion susceptibility of suspension bridge deck steels in the marine environment has been studied, and the results are displayed in Figure 11. It can be seen from this figure that based on the part of the calculation on the comparison of welded joints, the calculation results of WZ and HAZ are according to the measured gain. Besides, the WZ area is about 3 times of HAZ area, considering the BM's impossible unlimited extension influence on the HAZ, assumes that the BM area and HAZ area ratio is 3. Therefore, under the condition of the HAZ size is  $1\text{ cm}^2$ , transform the current density in Figure 10 to the electric current and potential curves in Figure 11 through the area ratio, thus obtained the coupling potential ( $E_{\text{couple}}$ ) from the WZ, BM, and HAZ zone. It can



TABLE 2: Tensile properties of bridge deck samples in service.

Number	Average thickness (mm)	Yield load (kN)	Ultimate load (kN)	Nominal yield stress (MPa)	Nominal tensile strength (MPa)	Elongation (%)
1-3	≈10.4	64.0	91.4	355	507	31
1-8	≈9.8	60.8	86.9	337	483	36
2-1	≈11.6	71.6	93.4	398	519	33
2-7	≈11.3	65.2	89.0	362	494	31
2-10	≈7.8	43.0	66.0	239	366	19
3-2	≈10.5	54.0	81.9	300	454	16
3-7	≈9.3	52.5	80.4	291	446	16

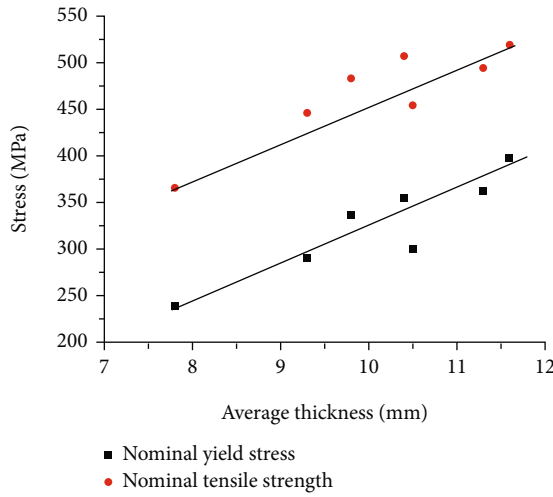


FIGURE 13: Nominal yield stress and tensile strength of specimens with the average thickness of specimens.

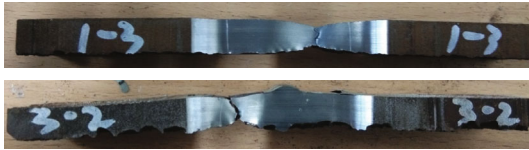


FIGURE 14: Images of the specimens and surface topography of the specimens with different corrosion state.

be seen that the coupling potential horizontal line and the HAZ anodic polarization curves are intersected at the point A, the current is about  $15 \mu\text{A}$  in point A, and the current value is 6.5 times better than the corrosion current density of HAZ (about  $2 \mu\text{A}$ ), indicating that the HAZ will be more fragile to the obvious galvanic corrosion accelerating effect during to the situation when WZ and the BM were accidentally coupling, and the results were correspond with the corroded contour image of HAZ in welded joints.

### 3.3. Tensile and Fatigue Test Results

**3.3.1. Tensile Test Results.** The typical nominal stress-strain curve is shown in Figure 12. The nominal stress of specimen refers to the load of the specimen divided by the initial area (the width  $\times$  the initial thickness (12 mm)) of the specimen. The tensile properties of samples with different corrosion

degrees are shown in Table 2. The variation of nominal yield stress and the nominal tensile strength with the average thickness of the specimens is shown in Figure 13. The nominal yield stress and the nominal tensile strength of the specimen decreased with the reduction of the sample average thickness.

$$\text{Nominal yield stress} = \frac{\text{yield load}}{(\text{sample width} \times \text{sample initial thickness (12 mm)})}$$

$$\text{Nominal tensile strength} = \frac{\text{ultimate tensile load}}{(\text{sample width} \times \text{sample initial thickness (12 mm)})} \quad (6)$$

From Table 2 and Figure 13, the average thickness of cross section of the samples 1-3 and 3-2 was similar, but the nominal yield stress and nominal tensile strength of the 3-2 samples are obviously lower. This is because the surface corrosion morphology can influence the nominal yield stress and nominal tensile strength. The morphology of corrosion pits on the sample surface is shown in Figure 14. Compared with the surface condition of samples 1-3 and 3-2, the size of the corrosion pit in sample 3-2 is larger. The corrosion pits act as a notch, and the larger the corrosion pit on the surface of the sample, the greater the influence on the tensile properties.

**3.3.2. Residual Fatigue Life Test Results.** The fatigue test results are shown in Table 3. The stress amplitude 115 MPa is the design stress amplitude of bridge deck. The relationship between the average thickness and fatigue life under nominal stress amplitude of 115 MPa is shown in Figure 15. With the increase of the corrosion degree of the samples, that is, the decrease of the average thickness of the sample, the actual stress amplitude of the sample increases under the same fatigue load amplitude.

As shown in Figure 15, the residual fatigue life decreases with the decrease of average thickness under nominal stress amplitude of 115 MPa. When the sample thickness is 10 mm, the sample has an infinite life, and when the thickness reached 9 mm, the fatigue life is lower than  $10^6$  cycles. This means that it no longer meets the design requirements. Therefore, in order to ensure the safety service of the bridge deck, the average thickness after corrosion should not be less than 10 mm.

The surface morphology and fracture position of the sample are shown in Figure 16. All the species were covered with



TABLE 3: Fatigue test results of bridge deck specimens.

Average thickness (mm)	Load amplitude (kN)	Actual stress amplitude (MPa)	Nominal stress amplitude (MPa)	Number of cycles (N)
≈6.0	20.7	230	115	$2.48 \times 10^4$
≈8.0	20.7	172	115	$1.94 \times 10^5$
≈9.0	15.5	115	86.1	$5 \times 10^6$
≈9.0	20.7	153	115	$6.43 \times 10^5$
≈10.0	20.7	138	115	$5 \times 10^6$
≈10.5	27.1	172	150	$2.68 \times 10^5$

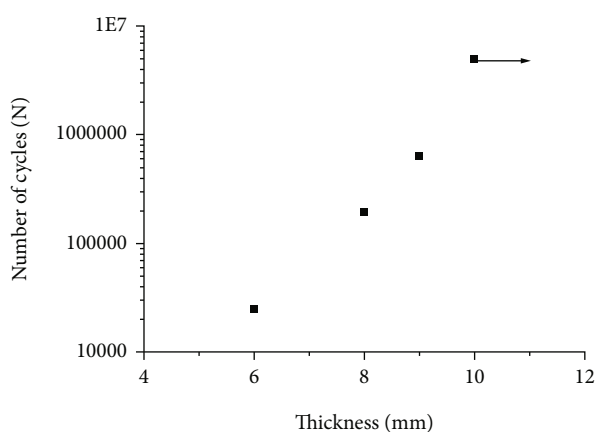


FIGURE 15: The variation of fatigue life with thickness under the nominal stress amplitude is 115 MPa.



FIGURE 16: Surface morphology of fatigue test samples cut from bridge deck.

etch pits. This agrees with reports that fatigue performance can be reduced by etch pits. For example, Song et al. [30] investigated the fatigue behavior of the different types of pits. Results indicate that corrosion pits reduce the fatigue life significantly, particularly the sharp pits and the interacting pits. A nondestructive methodology based on 3D profile data for fatigue life prediction has been presented. The predictions are shown to compare well against experimental results. Rahgozar and Sharifi [31] measured the fatigue performance of six

standard specimens which were taken from flanges and webs of three severely corroded steel beams that were recovered from a petrochemical site. The result shows that there is a reduction in fatigue life of corroded steel specimens with corrosion pitting that are due to the “notch factor” effect and indirectly yield a quantitative relationship between the pitting corrosion and the corresponding remaining fatigue life of a corroded steel structure.

#### 4. Conclusions

In this study, typical structure of welded joint samples obtained from suspension bridge was analyzed using macro and micro analysis equipment, and their corrosion and fatigue performance were tested. Some general results are summarized as follows:

- (1) The corrosion of the welded joint in the HAZ was serious, and the annual average corrosion rate reached 0.3-0.4 mm/y. There existed obviously local corrosion in both WZ and HAZ, and the depth pit in HAZ was about 1.8 mm, which has a high risk of local corrosion
- (2) The corrosion potential of the HAZ was the most negative in the welded joint, and the corrosion of HAZ was accelerated by the galvanic effect of WZ and BM. The corrosion current (about  $2 \mu\text{A}$ ) in the HAZ is increased by about 6.5 times under the condition of single corrosion
- (3) The elongation of the serviced specimens decreased by nearly 40% compared with samples without service, and the corrosion thinning and etch pits had a coupling effect on the decrease of the elongation
- (4) The nominal yield stress and tensile strength of the sample decreased with the reduction of the average thickness. The surface corrosion pits have a stress concentration effect similar to the notch, which reduced the plasticity and strength of the samples
- (5) In order to ensure the safety service of the bridge deck, the average thickness of the samples after corrosion should not be less than 10 mm

## Data Availability

The data used to support the findings of this study are available from the corresponding author upon request.

## Conflicts of Interest

The authors declare no financial or commercial conflict of interest.

## Authors' Contributions

Xudong Zhou and Xinmin Zhang were involved in conceptualization, investigation, writing—original draft, and project management. Ruiwen Xu and Bin Li were involved in investigation, data analysis, and review and editing. Xuechong Ren, Jinyang Zhu, and Ying Jin were involved in investigation and writing and review.

## References

- [1] Y. Xu, Y. Huang, F. Cai, D. Lu, and X. Wang, "Study on corrosion behavior and mechanism of AISI 4135 steel in marine environments based on field exposure experiment," *The Science of the Total Environment*, vol. 830, p. 154864, 2022.
- [2] M. A. Melia, J. G. Duran, J. M. Taylor, F. Presuel-Moreno, R. F. Schaller, and E. J. Schindelholz, "Marine atmospheric corrosion of additively manufactured stainless steels," *Corrosion*, vol. 77, no. 9, pp. 1003–1013, 2021.
- [3] X. Yang, J. Yang, Y. Yang et al., "Data-mining and atmospheric corrosion resistance evaluation of Sn- and Sb-additional low alloy steel based on big data technology," *International Journal of Minerals, Metallurgy, and Materials*, vol. 29, no. 4, pp. 825–835, 2022.
- [4] W. Sun, C. Xing, X. Tang, Y. Zuo, Y. Tang, and X. Zhao, "Comparative study on the degradation of a zinc-rich epoxy primer/acrylic polyurethane coating in different simulated atmospheric solutions," *Journal of Coating Technology and Research*, vol. 18, no. 2, pp. 397–413, 2021.
- [5] L. Pang, Z. Wang, Y. Zheng, X. Lai, and X. Han, "On the localised corrosion of carbon steel induced by the in-situ local damage of porous corrosion products," *Journal of Materials Science & Technology*, vol. 54, no. pre-published, pp. 95–104, 2020.
- [6] X. Liao, B. Qiang, J. Wu, C. Yao, X. Wei, and Y. Li, "An improved life prediction model of corrosion fatigue for T-welded joint," *International Journal of Fatigue*, vol. 152, no. 6, Article ID 106438, 2021.
- [7] H. Ma, J. Zhao, Y. Fan et al., "Comparative study on corrosion fatigue behaviour of high strength low alloy steel and simulated HAZ microstructures in a simulated marine atmosphere," *International Journal of Fatigue*, vol. 137, p. 105666, 2020.
- [8] H. S. Klapper, C. Menendez, and S. Jesse, "Pitting corrosion resistance influencing corrosion fatigue behavior of an austenitic stainless steel in chloride-containing environments," *Corrosion*, vol. 76, no. 4, pp. 398–410, 2020.
- [9] P. Qvale, H. O. Nordhagen, S. K. Ås, and B. H. Skallerud, "Effect of long periods of corrosion on the fatigue lifetime of offshore mooring chain steel," *Marine Structures*, vol. 85, article 103236, 2022.
- [10] Y. F. Ma, Y. Xiong, Z. G. Chen et al., "Effect of surface nanocrystallization produced by laser shock processing on the corrosion fatigue behavior of 300M steel," *Surface & Coatings Technology*, vol. 439, p. 128426, 2022.
- [11] Y. Guo, Y. Shao, X. Gao, T. Li, Y. Zhong, and X. Luo, "Corrosion fatigue crack growth of serviced API 5L X56 submarine pipeline," *Ocean Engineering*, vol. 256, article 111502, 2022.
- [12] Z. Li, D. Fu, Y. Li et al., "Application of an electrical resistance sensor-based automated corrosion monitor in the study of atmospheric corrosion," *Materials*, vol. 12, no. 7, p. 1065, 2019.
- [13] M. Głuszko, "Corrosion hazard of energetic lines exploited area in atmospheric conditions," *Przegląd Elektrotechniczny*, vol. 87, no. 2, 2011.
- [14] M. Morcillo, I. Diaz, and H. Cano, "Atmospheric corrosion of mild steel," *Revista De Metalurgia*, vol. 47, no. 5, pp. 426–444, 2011.
- [15] A. Nakano, W. Oshikawa, and N. Yonezawa, "Evaluation of corrosion properties of steel with Zn-30 mass% Al thermal-spray coating using accelerated atmospheric exposure test," *Materials Transactions*, vol. 62, no. 7, pp. 1001–1008, 2021.
- [16] D. G. Manning, "Corrosion performance of epoxy-coated reinforcing steel: North American experience," *Construction and Building Materials*, vol. 10, no. 5, pp. 349–365, 1996.
- [17] S. Li and L. H. Hihara, "In situ Raman spectroscopic study of NaCl particle-induced marine atmospheric corrosion of carbon steel," *Journal of the Electrochemical Society*, vol. 159, no. 4, pp. C147–CC54, 2012.
- [18] Y. S. Kim and J. G. Kim, "Corrosion behavior of pipeline carbon steel under different iron oxide deposits in the district heating system," *Metals*, vol. 7, no. 5, p. 182, 2017.
- [19] C. J. Yi, "Durability study of reinforced concrete bridge," *Applied Mechanics and Materials*, vol. 204, pp. 2061–2064, 2012.
- [20] S. H. Xu and Y. D. Wang, "Estimating the effects of corrosion pits on the fatigue life of steel plate based on the 3D profile," *International Journal of Fatigue*, vol. 72, pp. 27–41, 2015.
- [21] D. J. Thomas, "A life at sea and the corrosion fatigue lives of offshore structures," *Journal of Failure Analysis and Prevention*, vol. 21, no. 3, pp. 707–710, 2021.
- [22] X. Xu, Z. Liu, T. Zhao, Q. Cui, T. Zhang, and X. Li, "Corrosion fatigue behavior of Fe-16Mn-0.6C-1.68Al twinning-induced plasticity steel in simulated seawater," *Corrosion Science*, vol. 182, p. 109282, 2021.
- [23] G. W. Yao, S. C. Yang, J. Q. Zhang, and Y. L. Leng, "Analysis of corrosion-fatigue damage and fracture mechanism of in-service bridge cables/hangers," *Advances in Civil Engineering*, vol. 2021, Article ID 6633706, 10 pages, 2021.
- [24] Q. Xu, F. Shao, L. Y. Bai, Q. N. Ma, and M. Shen, "Corrosion fatigue crack growth mechanisms in welded joints of marine steel structures," *Journal of Central South University*, vol. 28, no. 1, pp. 58–71, 2021.
- [25] G. Yao, X. Yu, L. Gu, and Y. Jiang, "Experiment on corrosion fatigue life of steel strands under the coupling effects of chloride environment and alternating loads," *Advances in Civil Engineering*, vol. 2021, Article ID 2439503, 12 pages, 2021.
- [26] X. Liao, Y. Li, B. Qiang, J. Wu, C. Yao, and X. Wei, "An improved crack growth model of corrosion fatigue for steel in artificial seawater," *International Journal of Fatigue*, vol. 160, article 106882, 2022.
- [27] V. Krivy, M. Kubzova, K. Kreislova, and V. Urban, "Characterization of corrosion products on weathering steel bridges

- influenced by chloride deposition,” *Metals*, vol. 7, no. 9, p. 336, 2017.
- [28] T. Zhang, W. Liu, B. Dong et al., “Investigation on the nickel content design and the corrosion resistance of low alloy steel welded joint in tropical marine atmosphere environment,” *Materials and Corrosion*, vol. 72, no. 10, pp. 1620–1634, 2021.
- [29] Y. L. Huang, D. Yang, Y. Xu, D. Z. Lu, L. H. Yang, and X. T. Wang, “Field study of weather conditions affecting atmospheric corrosion by an automobile-carried atmospheric corrosion monitor sensor,” *Journal of Materials Engineering and Performance*, vol. 29, no. 9, pp. 5840–5853, 2020.
- [30] F. M. Song, D. W. Kirk, J. W. Graydon, and D. E. Cormack, “Effect of ferrous ion oxidation on corrosion of active iron under an aerated solution layer,” *Corrosion*, vol. 58, no. 2, pp. 145–155, 2002.
- [31] R. Rahgozar and Y. Sharifi, “Remaining fatigue life of corroded steel structural members,” *Advances in Structural Engineering*, vol. 14, no. 5, pp. 881–890, 2011.